OFF-DESIGN MODELING AND PERFORMANCE ASSESSMENT OF A THERMALLY INTEGRATED 6 KWE PUMPED THERMAL ENERGY STORAGE SYSTEM USING A REVERSIBLE ORC/HP

Neven Elise[1]*, Chaudoir Basile[1], Peeters Marie[1], Thomé Olivier[1], Dumont Olivier[1], Lemort Vincent[1]

[1] Thermodynamics Laboratory, University of Liege, Liege, Belgium

*Corresponding Author: elise.neven@uliege.be

ABSTRACT

This study explores the development of an off-design model of a 6 kWe thermally integrated pumped thermal energy storage system using a reversible organic rankine cycle/heat pump. Thermally integrated pumped thermal energy provides a promising solution to close the gap between energy supply and demand caused by the increasing production of renewable energy. The reversible nature of the proposed design allows for component reuse, reducing both costs and complexity. Additionally, the thermal integration of the system leverages low-temperature heat sources, such as district heating, to enhance operational flexibility. The focus of this research is the creation of an off-design model to assess the performances of the system under varying external conditions, including fluctuating district heating and storage temperatures, as well as ambient temperature. Detailed component models are developed, and a comprehensive system model is established for both heat pump and organic rankine cycle operating modes. Using this detailed model, performance maps of the system are generated by simulating its operation across defined boundary conditions. These performance maps serve as a guideline for system behavior under varying conditions and help define the operating range of the test bench before conducting the initial experimental tests.

1 INTRODUCTION

The growing share of renewable energy sources poses challenges for energy flexibility. Electrical Energy Storage (EES) is a key driver for bridging the gap between generation and demand of electricity (Chen *et al*., 2009). Amongst EES, Carnot Batteries (CB), also known as Pumped-Thermal Energy Storage (PTES), is an emerging technology that is designed to meet these challenges. PTES operates by using a Heat Pump (HP) to convert excess of electricity into heat, store it in a thermal storage, and then convert it back into electricity through a Heat Engine (HE).

The concept of Thermal Integration with PTES (TI-PTES) combines electrical and thermal energy input and output, which makes it the ideal link between different energy sectors, such as electricity and heat. According to demand and available resources, this flexibility allows for the best possible energy management for both heating and electricity (Steinmann *et al.* 2019). PTES can be incorporated into thermal systems in a number of ways, such as using solar thermal collectors, supporting district heating networks (DHNs), recovering waste heat, and drawing from geothermal wells (Hu *et al.* 2021).

Vapor compression heat pumps (VCHP) and organic Rankine cycles (ORC) are used in many TI-PTES applications that operate at relatively low temperatures (below 200°C). Both electrical and thermal inputs can power them, with the thermal input usually falling between 70°C and 100°C (Frate *et al.*, 2020).

To reduce equipment costs and improve economic viability, TI-PTES systems can use a reversible cycle, where the same components are used in both the charging (HP) and discharging (HE) phases. This approach is particularly well-suited for PTES, as the HP and HE modes never operate simultaneously, unlike in many other systems. However, for this design to be feasible, the thermal power levels of the HP and ORC must be similar to ensure comparable Reynolds numbers, which helps maintain efficient heat exchange in the heat exchangers. Additionally, in reversible HP/ORC systems that use reversible volumetric machines, it is essential to verify that the machine's volume ratio remains

within an acceptable range to match the cycle conditions and prevent performance losses (Dumont, 2017).

This paper examines a TI-PTES system that integrates a reversible ORC/VCHP with the DHN of the University of Liège. The reversible configuration enables the use of the same heat exchangers in both ORC and HP modes, as well as shared scroll compressors/expanders. A thermocline storage system is also used for thermal energy storage.

Despite the potential advantages of TI-PTES, its part-load performance remains largely unexplored (Frate et al., 2020). This study introduces an off-design model to evaluate the system's behavior under partial load conditions and optimize its operation in response to varying external factors. The model incorporates detailed component representations, calibrated with manufacturer data to ensure accuracy beyond nominal operating points. Additionally, it accounts for the energy consumption of auxiliary components, such as water pumps and the dry cooler's fan, which are often overlooked in performance assessments. Based on the results, several operational guidelines are provided to improve system control and efficiency in real-world applications. The goal of the off-design model is to offer guidance before the first operation of the test bench and to understand the system's operating range.

2 CASE STUDY

This section provides an overview of the system under study and details the methodology used for component sizing.

2.1 Description of the TI-PTES plant layout

The system studied is a TI-PTES plant using a reversible HP/ORC, combined with a thermocline for thermal storage. The plant is thermally integrated with the DHN of the main campus of the University of Liège, which serves as a heat source for the HP. This integration enhances the system's efficiency by improving the Coefficient of Performance (COP) of the HP. The thermal storage can directly supply heat to the DHN during peak demand, reducing the size of the DHN substation. (Poletto *et al.,* 2024). The system is represented in Figure 1 where DHN+ refers to the district heating supply line while DHN- to the district heating return line.

The unit comprises three constant-speed scroll machines operating in parallel, allowing capacity modulation in both HP and ORC modes. The heat exchangers (HX1 and HX2) keep on working at low pressure and high pressure respectively when switching from HP to ORC mode. The system offers three operational modes: thermal charge, electrical discharge, and thermal discharge.

In thermal charge mode (HP mode, represented by green arrows in Figure 1), the system extracts heat from the DHN. HX1 functions as a condenser, while HX2 serves as an evaporator. The scroll machines operate as compressors, and the pump and dry cooler lines are bypassed through a play of valve.

In electrical discharge mode (ORC mode, represented by purple arrows in Figure 1), the stored thermal energy is converted into electricity. The thermal storage discharges heat, thus HX1 acts as an evaporator while HX2 acts as a condenser. The scroll machines function as expander, while the expansion valve line is bypassed. The heat released by the condenser is then dissipated through the dry cooler.

Finally, in thermal discharge mode (represented by red arrows), the system directly transfers heat from the thermal storage to the DHN.

In a reversible system like this, controlling the refrigerant charge is crucial, as shown by Tassenoy *et al.* (2022) and Weitzer *et al.* (2023). The system operates with a higher charge in ORC mode and a lower charge in HP mode. In HP mode, the charge automatically adjusts by flowing through the liquid receiver (LR). In ORC mode, the charge can be increased by closing the valve next to the LR while opening other valves to pump refrigerant from the LR. To return refrigerant to the LR, the valve next to the LR is opened while the valve next to the expansion valve is closed.

2.2 TI-PTES design and sizing

Based on the case study, the system must be properly sized to meet the power and energy requirements at the given temperature levels, ensuring the selection of suitable components for the plant. To achieve this, an on-design model is used to evaluate different system configurations and determine the optimal setup. The detailed methodology for system sizing is presented by Dumont *et al.* (2023), this section provides a summary of the key principles applied.

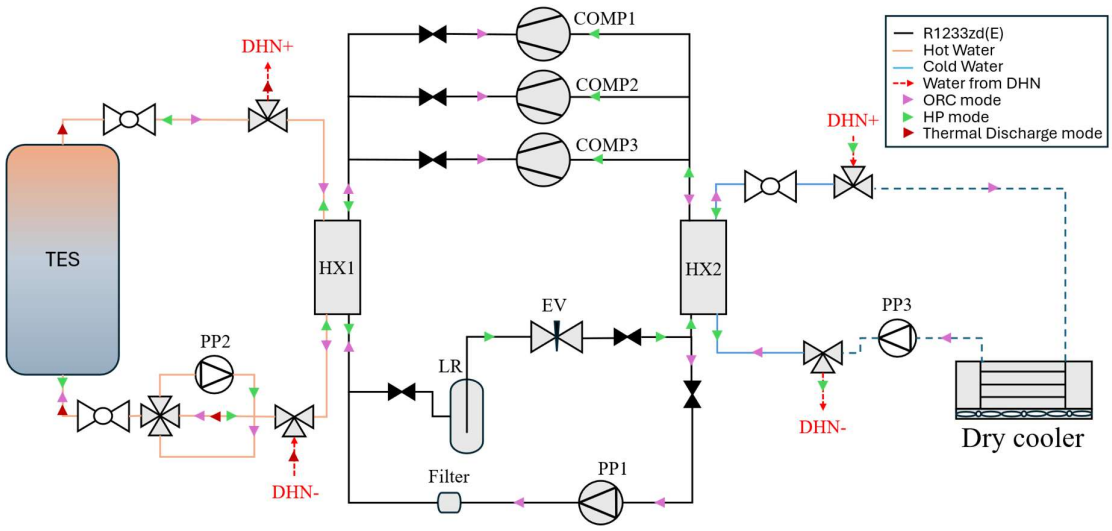

Figure 1: TI-PTES plant layout.

The sizing and modelling of the prototype were carried out according to the following criteria:

- The system is primarily sized based on thermal discharge mode, as peak thermal demand occurs every morning for 15 minutes, whereas electrical peaks are shorter and less frequent. The hot water storage tank is designed to supply 400 kW of thermal power for 15 minutes, requiring a total storage capacity of 100 kWh for a temperature range of 63°C to 77°C, corresponding to the mean supply and return temperatures of the DHN. This results in a required hot water tank volume of 6.1 m^3.
- The HP is sized to fully recharge the thermal storage within 1.5 hours, requiring a condenser power of about 80 kW (the storage is slightly over sized).
- The ORC system is sized to ensure that the Reynolds number at the expander outlet in ORC mode is of the same order of magnitude as that at the compressor inlet in HP mode. These locations are selected because they correspond to the highest pressure loss points in the system. Maintaining similar Reynolds numbers helps achieve comparable flow conditions, ensuring high performance in both HP and ORC operations (Dumont, 2017). Based on this criterion, the evaporator power is set to 100 kW, resulting in an estimated discharge time of approximately one hour.
- R1233zd was chosen as the working fluid due to its superior performance in both HP and ORC modes.
- The dry cooler is designed to dissipate the entire thermal power output of the ORC condenser.

The design values are derived from the on-design model (Table 1).

Table 1: Sizing of the components.

Mode	Charge – HP	Discharge – ORC
Thermal energy [kWh]	124	100
Electrical energy [kWh]	16	5.6
Time of charge/discharge [h]	1.5	1
Electrical power [kW]	10.7	5.6
Condenser power [kW]	82.5	94.6
Evaporator power [kW]	67.3	100
Condenser pressure [bar]	6.02	1.18
Evaporator pressure [bar]	3.34	4.05
Cold temperature [°C]	62	20
Hot temperature [°C]	76	70
COP/eta [-]	7.69	5.5
Condenser flow (sf) [l/s]	1.4	2.6
Evaporator flow (sf) [l/s]	3.2	2.6

Optimal volume ratio [-]	1.68	3.04
Working fluid mass flow rate [kg/s]	0.422	0.499

Manufacturers can provide the components using the values in Table 1 (Table 2).
The available swept volumes of the scroll compressors were lower than those predicted by the on-design model. To compensate for this, three scroll compressors were arranged in parallel. Since the swept volume in expander mode (ORC mode) is lower than in compressor mode (HP mode), the system operates with two scroll compressors in HP mode and three scroll expanders in ORC mode at the nominal operating point to maintain the required pressure levels.
Additionally, to further compensate for the lower swept volume, the mass flow rate is increased by running the scroll machines at their maximum speed (6000 RPM) in both modes. As the system lacks an inverter, the rotational speed is fixed and dictated by the pulley ratio between the scroll machine and the motor/generator.

Table 2: Selected components.

Component	Product
Refrigerant pump	SAWA peripheral pump MP73-RKFE
High pressure heat exchanger	SWEP P200TH 140 plates
Low pressure heat exchanger	SWEP P200TH 140 plates
Expansion valve	Danfoss ICM 20-B
Volumetric machines	SANDEN scroll compressor
Dry cooler	Aia XPS (2 fans)
Thermal storage	$7m^3$ tank

3 METHODOLOGY AND MODELLING

After sizing the system, it is essential to analyze its behavior outside the nominal operating point. However, the previously described on-design model is not suitable for assessing non-nominal conditions. To address this, an off-design model is developed to accurately characterize the system's behavior under varying operating conditions. This detailed model provides a more realistic assessment of off-design performance, allowing for more accurate extrapolation of system behavior.
The following section outlines the methodology used for off-deign modelling. Two separate models are implemented: one for the ORC unit and one for the HP unit. The model is developed in Python and follows the architecture of the *LaboThapPy* library.
The objective is not to achieve highly precise system simulations but rather to gain an initial understanding of the operating range of the test bench in both HP and ORC modes before its operation. Additionally, the model provides valuable insights into system behavior under different boundary conditions.

3.1 Components models

To perform off-design simulations, the model is built using well-established physical component models, which have been widely validated in the literature for accurately representing off-design behavior. The main source of uncertainty lies in the selection of parameter values rather than the component models themselves. This section describes the modeling approach used for the different components.
In both HP and ORC modes, the system operates with two heat exchangers that alternate between functioning as condensers and evaporators, depending on the mode. In both cases, the working fluid undergoes phase change within both the evaporator and condenser, resulting in multiple fluid states (liquid, two-phase, and vapor) coexisting within a single component. To accurately capture the heat transfers, the heat exchangers models are divided into several zones.
To account for this division, a moving-boundary model is chosen to simulate the heat exchanger. The model is based on the generalized moving boundary algorithm proposed by Bell *et al.* (2015) and later reimplemented by Dickes *et al.* (2018). However, the accuracy of this model heavily depends on the proper identification of heat transfer coefficients, as it is highly sensitive to the chosen correlations.
The following heat transfer correlations are used to model the heat exchangers:

- Martin Holger correlation for single-phase R1233zd(E) flow (VDI Atlas).

- Correlation proposed by Shah (2021) for R1233zd(E) condensation.
- Amalfi (2003) correlation for R1233zd(E) evaporation.

These correlations are calibrated using certain geometric parameters of the heat exchangers that are not provided in the manufacturer's datasheet, such as casing thickness, amplitude of the sinusoidal corrugation pattern, chevron angle, plate thickness, and corrugation pitch. The initial calibration is performed using one data point from the manufacturer, specifically heat transfer rates and the heat transfer coefficients. However, a single calibration point is insufficient, and further refinement will be required using experimental data from the test bench. Additionally, since both heat exchangers alternate between condenser and evaporator roles depending on the mode, this behavior may further influence the heat transfer correlations.

The volumetric machines are modeled using semi-empirical models. These models rely on a limited set of key equations to capture the most significant physical phenomena occurring within the process. This modeling approach provides a balance between calibration effort, simulation speed, accuracy, and extrapolation capability. The scroll compressor and expander are simulated using the grey-box model proposed by Lemort *et al*. (2009). This model accounts for various operational factors, including;

Under- and over- expansion/compression, heat transfers and pressure drops at the inlet and outlet ports, mechanical losses, internal leakages and heat losses to the environment. The model parameters are calibrated using experimental data provided by the manufacturer.

The refrigerant pump and the water pumps are modeled using the characteristic curves provided by the manufacturer.

The liquid receiver is a single tank placed at the condenser outlet in the HP mode. It is considered thermodynamically passive for the working fluid and its behavior is described by the following equations:

$$h_{su,LR} = \mathrm{h}_{\mathrm{ex,LR}} \quad (1)$$

$$P_{su,LR} = P_{ex,LR} \quad (2)$$

This configuration ensures that the working fluid remains in a saturated liquid state at the condenser outlet, thereby enforcing the subcooling to zero ($\Delta T_{sc} = 0$).

The expansion valve is modeled as a simple isenthalpic process.

Pressure drops in the system are currently neglected; however, they will need to be considered, as they play a significant role. The prototype was designed to minimize pressure losses, ensuring optimal performance.

The dry cooler is modeled as a water-air heat exchanger, with the air mass flow rate specified in the manufacturer's datasheet.

A simple epsilon-NTU model is used for simulation, considering only forced convection at this stage.

The thermocline is not considered in this study, as its dynamic behavior can no longer be neglected. Instead, only the possible hot and cold temperatures within the thermocline are simulated.

In Table 3, the different models of component are stated.

Table 3: Component models.

Component	Model
Refrigerant pump	Based on characteristic curve
Heat exchangers	Moving-boundary model (Bell *et al.,* 2015)
Scroll volumetric machines	Semi-empirical model (Lemort *et al.,* 2009)
Dry cooler	Epsilon-NTU model
Water pumps	Based on characteristic curves

3.2 System modelling methodology

To model the system, the individual component models are interconnected. This is done using the *LaboThapPy* library's solving approach.

The methodology is as follows: each component is linked to another through a "connector", which represents an energy flow between components. A connector can transfer energy in the form of mass, heat, or work. In this application, the components are connected using "mass connectors", which transfer energy via fluid flow between components.

The system consists of three separate circuits, each characterized by a different working fluid:

1. Refrigerant circuit (ORC or HP)
2. Hot water circuit
3. Cold water circuit

These circuits are interconnected through shared components, specifically the evaporator and condenser, ensuring the energy exchange between the circuits.

3.3 ORC system modelling

As explained in the previous section, the ORC system model is composed of three separate circuits: the refrigerant circuit, hot water circuit, and cold water circuit, as illustrated in Figure 2.

The inclusion of the secondary circuits (hot and cold water loops) is essential, as accounting for the auxiliary energy consumption—such as that of the water pumps and dry cooler—significantly impacts the overall system performance.

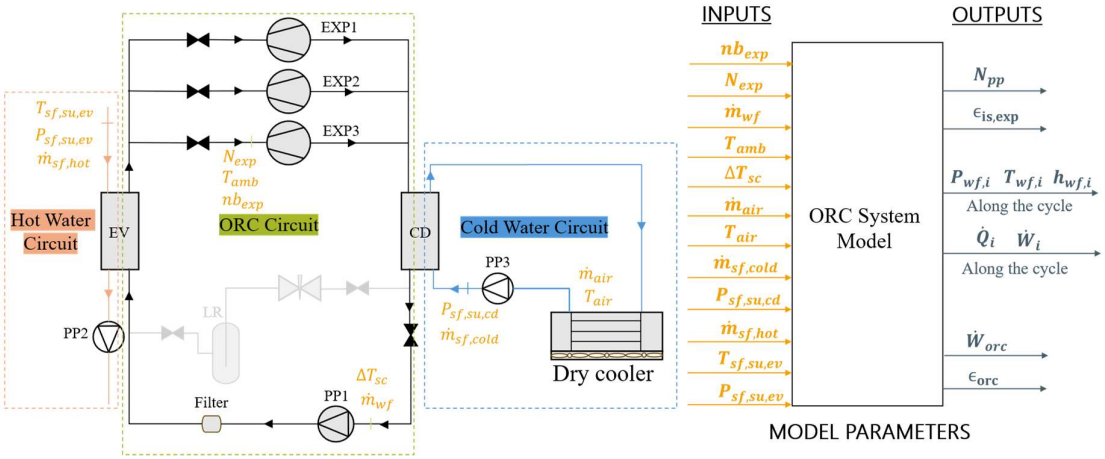

Figure 2: ORC mode layout (Right) and information diagram of ORC system model (Left).

In Figure 2 (right), the complete system is illustrated, with model inputs highlighted in orange. The thermocline is not explicitly represented, as only the storage outlet temperature affects the system's steady-state behavior. Consequently, the storage high temperature serve as inputs to the model.

In Figure 2 (left), an information diagram illustrates the inputs, outputs, and parameters of the model. The ORC system model is designed so that its performance is solely determined by its boundary conditions and an imposed subcooling, which are set to match the actual conditions the test rig will experienced. These boundary conditions are further investigation in section 4.1. The number of fans turned on is also an input of the system, so far both fans are assumed to be turned on.

To solve the entire system, each circuit is computed individually. The ORC circuit serves as the main solver. When a component belonging to another circuit is encountered, that circuit is solved first before proceeding with the ORC circuit. For example, when the solver reaches the condenser, it first computes the cold water circuit before continuing with the rest of the ORC system.

The ORC circuit solver operates as follows. Since the thermodynamic state of the system cannot be determined directly, it is found through an optimization process that minimizes internal modelling residuals. Specifically, the ORC model iterates on the supply and exhaust pump pressures until the residuals (Equations (1) and (2)) fall below a predefined threshold ($\mathbf{10^{-3}}$).

$$res_1 = 1 - \frac{N_{exp,calc}}{N_{exp,input}} \quad (1)$$

$$res_2 = 1 - \frac{h_{cd,ex,calc}}{h_{su,pp}} \quad (2)$$

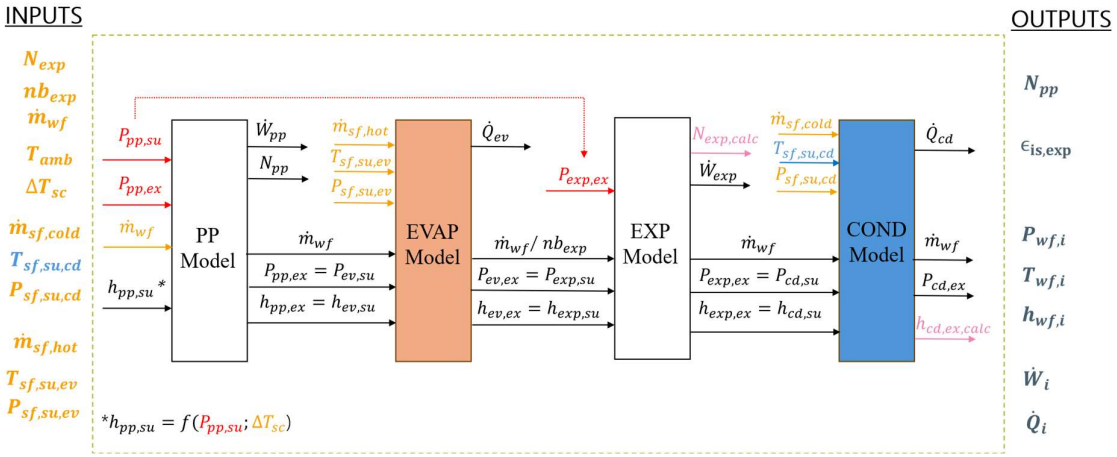

Figure 3: Solver architecture of the ORC circuit. System inputs are in orange, guesses in red, inputs calculated in the cold water circuit in blue, and values used to determine residuals in pink.

The ORC circuit solver, illustrated in Figure 3, follows the approach used by Dickes et al. (2018) and serves as the main solver. When the evaporator model is encountered, the hot water circuit is solved. This process is straightforward, with the water pump model being solved afterward to determine the pump's electrical consumption.

Similarly, when the main solver reaches the condenser, it first solves the cold water circuit. Since the inlet temperature of the cold water entering the condenser is initially unknown, an iterative process is required to determine it based on the air temperature and the dry cooler model (Figure 4).

The solver updates the cold water inlet temperature at the condenser with the value calculated at the dry cooler outlet, repeating this process until convergence is achieved. Once the cold water circuit is solved, the main solver updates the pressure estimates and continues iterating until overall convergence is reached.

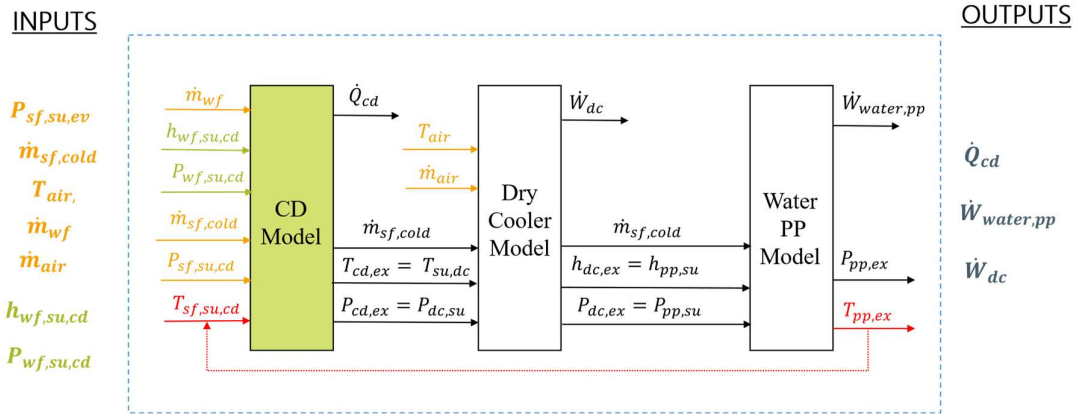

Figure 4: Solver architecture of the Cold Water circuit.

3.4 HP system modelling

Figure 5 illustrates the system in HP mode. The same solver approach used for the ORC system is applied here. The HP system is also solved by decomposing it into three separate circuits, each representing a different fluid. Similar to the ORC system model, the HP system model is structured so that its performance is determined by its boundary conditions and the subcooling. The boundary conditions are explained in section 4.1.

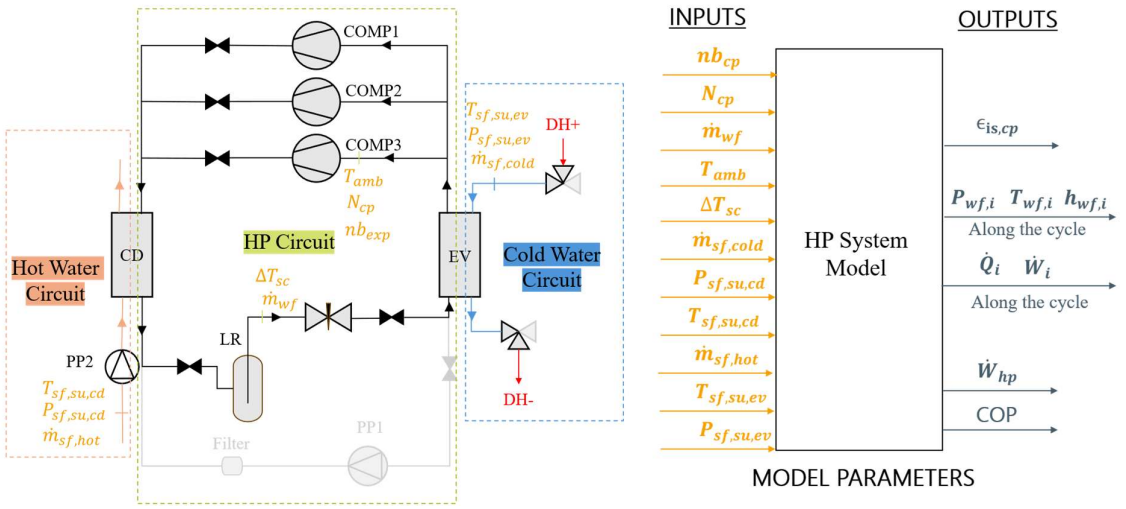

Figure 5: HP mode layout (Right) and information diagram of HP system model (Left).

The HP circuit also serves as the main solver. The HP model iterates on the supply and exhaust expansion valve pressures and the residuals are determined with Equations (3) and (4).

$$res_1 = 1 - \frac{N_{cp,calc}}{N_{cp,input}} \tag{3}$$

$$res_2 = 1 - \frac{h_{ex,cd,calc}}{h_{su,vlv}} \tag{4}$$

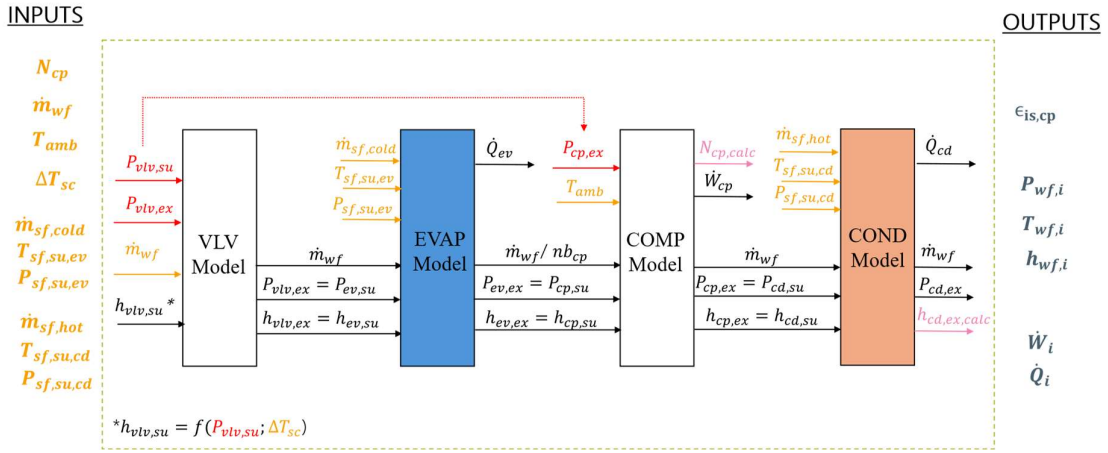

Figure 6: Solver architecture of the HP circuit. System inputs are in orange, guesses in red, and values used to determine residuals in pink.

The main solver (HP circuit) is depicted in Figure 6 and follows the same structure as the ORC's solver. The cold and hot water circuit solvers are straightforward and do not require iterations; only the pump consumptions are determined in both circuits.

3.5 Key performance indicators

To characterize the system in ORC and HP modes, two key parameters are used: the COP of the HP (Equation (5)) and the ORC efficiency (Equation (6)). The ORC efficiency accounts for auxiliary consumption, as these energy consumptions are not negligible.

$$COP = \frac{\dot{Q}_{cd}}{\dot{W}_{tot}} = \frac{\dot{Q}_{cd}}{\dot{W}_{cp,el} + \dot{W}_{pp,aux,el}} \tag{5}$$

$$\eta = \frac{\dot{W}_{tot}}{\dot{Q}_{ev}} = \frac{\dot{W}_{exp,el} - \dot{W}_{pp,el} - \dot{W}_{pp,aux,el} - \dot{W}_{dc}}{\dot{Q}_{ev}} \tag{6}$$

4 RESULTS AND DISCUSSION

To better understand the system's behavior under different boundary conditions, the system's model is used to evaluate the performance under varying boundary conditions.

4.1 Boundary conditions

The boundary conditions can be classified into two categories (Dickes, 2019): external variables and internal variables.

For the ORC system, the high temperature of the thermal storage and the air temperature are considered external variables, as they cannot be influenced by the ORC operation. In contrast, the rotational speeds of the refrigerant pump (PP1) and of the water pumps (PP2 and PP3) are internal variables that can be adjusted to influence system performance. The mass flow rates can be derived directly from the speeds. The scroll expander/compressor speed is fixed at 6000 RPM, this avoids the need for expensive power electronics. Additionally, the number of active scroll units can be adjusted.

The number of fans in the dry cooler is another adjustable variable. However, the fan speed (and thus the air mass flow rate) remains fixed, meaning fans can only be turned on or off.

The refrigerant charge is not yet considered in the model, it will play a significant role in future refinements. In Table 4, the boundary conditions of the ORC system are stated.

Table 4: Boundary conditions of the ORC.

Variable	Design	Min.	Max.	Unit
External variables				
Hot water temperature	76	45	95	°C
Ambient air temperature	15	-15	45	°C
Internal variables				
Refrigerant mass flow rate	0.499	0.1	1.6	kg/s
Cold water mass flow rate	2.6	1	7	kg/s
Hot water mass flow rate	3.2	1	11	kg/s
Number of expanders	3	1	3	-
Number of fans	2	0	2	-
Fixed variables				
Air flow rate of the fans	3.22			m^3/s
Speed of expander	6000			RPM

For the HP system, the low temperature of the thermal storage, the temperature from the DHN supply line, and the mass flow rate from the DHN are considered external variables, as they cannot be controlled by the system.

The refrigerant mass flow rate, however, is regulated by the expansion valve opening, making it an internal variable. Similarly, the speed of the water pump in the hot water circuit is also an internal variable that can be adjusted to influence system performance. The boundary conditions of the HP mode are stated in Table 5.

Table 5: Boundary conditions of the HP.

Variable	Design	Min.	Max	Unit
External variables				
Cold water temperature (DH+)	62	35	80	°C
Cold water mass flow rate	1.4	0.5	5	kg/s
Hot water temperature	76	50	95	°C
Internal variables				
Refrigerant mass flow rate	0.422	0.1	1.6	kg/s
Hot water mass flow rate	3.2	1	11	kg/s
Number of compressors	2	1	3	-
Fixed variables				
Speed of compressors	6000			RPM

4.2 Performance maps

Once the boundary conditions are defined, the system model is executed for both HP and ORC applications. The objective is to analyze the system's behavior under various external variables combination and identify any operational limits.

First, the performance in ORC mode is analyzed. Figure 7 presents an example of a performance map, where the heat source temperature (from the storage) is set to 90°C and the air temperature to 5°C. Due to the high number of internal variables (five), it is not feasible to represent the impact of all variables simultaneously. The graphs focus on the effects of the refrigerant mass flow rate and the hot water mass flow rate on the ORC efficiency and power output. In this case, the number of expanders is fixed at two, the cold mass flow rate is set to 3 kg/s, and both fans are fully operational.

These graphs enable the identification of the optimal operating point for the given set of external variables. Two types of optimization can be performed: full load and part load. In full load operation, the objective is to maximize net power generation, whereas in part-load operation, the ORC's performance is constrained by the amount of available energy in the heat source. In this case, the system should not be operated to maximize power output but rather to optimize efficiency (Dickes, 2019).

In Figure 7(a), the point that maximizes efficiency is shown, while Figure 7(b) illustrates the point that maximizes power output.

It can be observed that the ORC efficiency and the total work output are primarily dependent on the working fluid mass flow rate.

In the discharge mode of a PTES, a limitation may be imposed on the heat extracted from the thermal storage to discharge it within a specific timeframe. This imposes a limit on the thermal power at the evaporator. In such a case, the system operates in part-load mode, aiming to maximize efficiency for a given power at the evaporator. This is demonstrated in Figure 7a, where iso-evaporator capacity lines are shown. When the working fluid mass flow rate is much lower than that of the hot water, the iso-evaporator capacity lines appear vertical, as heat transfer is limited by the working fluid side.

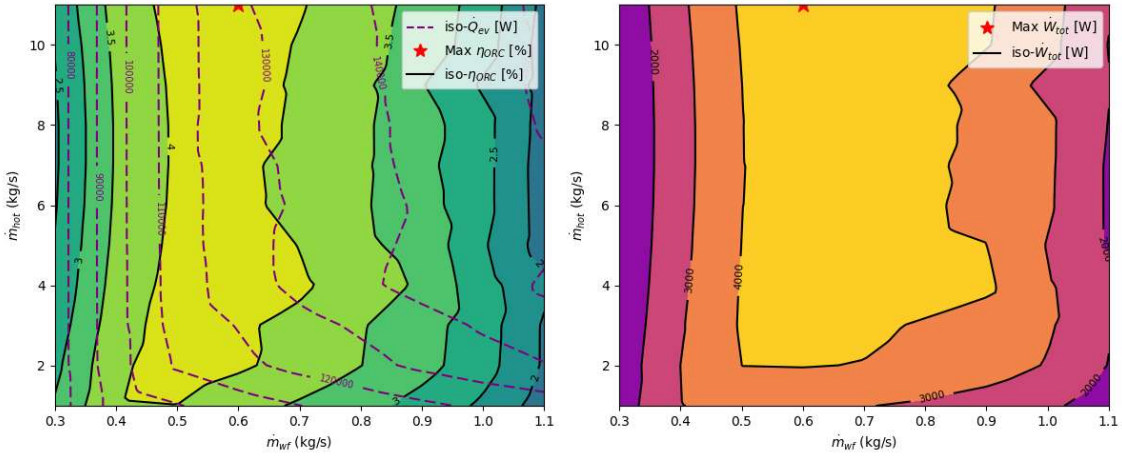

Figure 7: ORC performance maps for a $T_{hot} = 90$°C and $T_{air} = 5$°C, $\dot{m}_{cold}$ = 3 kg/s, with two expanders working in parallel and both fans activated. (a) η_{ORC} [%] as a function of $\dot{m}_{wf}$ and $\dot{m}_{hot}$. (b) $\dot{W}_{tot}$ [W] as a function of $\dot{m}_{wf}$ and $\dot{m}_{hot}$.

In HP mode, the same optimization principle applies. For each combination of external variables, an optimal set of internal variables can be identified. The maps in Figure 8 are generated for a storage temperature of 76°C and a cold water temperature of 62°C from the DHN, with a cold mass flow rate of 3 kg/s and two compressors.

The optimal operating points in Figure 8 can be identified based on two different objectives: maximizing the thermal power output at the condenser for full-load operation or maximizing the COP for efficient part-load operation. Initially, the system operates at maximum capacity to charge the thermal storage as quickly as possible. However, as the storage approaches full charge, the heat pump power is gradually reduced, shifting the focus from maximizing output to optimizing efficiency by operating at the highest possible COP for a given thermal power at the condenser (Padullés *et al.,*

2025). While the COP and thermal power primarily depend on the working fluid mass flow rate, the hot water mass flow rate must be sufficient to ensure effective condensation in the condenser.

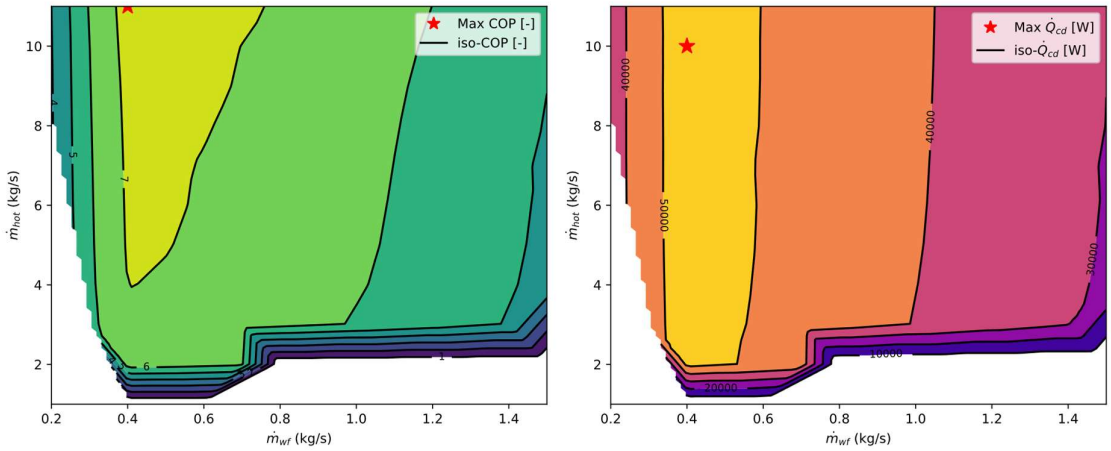

Figure 8: HP performance maps for a $T_{hot} = 76$°C and $T_{cold} = 62$°C, $\dot{m}_{cold}$ = 3 kg/s, with two compressors working in parallel. (a) COP [-] as a function of $\dot{m}_{wf}$ and $\dot{m}_{hot}$. (b) $\dot{Q}_{cd}$ [W] as a function of $\dot{m}_{wf}$ and $\dot{m}_{hot}$.

Those kind of maps should be simulated for all operating conditions, to obtain a matrix of optimum operation for the test bench.

The optimal control strategy should be defined by a higher-level optimization approach, such as the one proposed by Poletto *et al*. (2024), which considers electricity prices and forecasts energy demand. These higher control levels determine whether the system should operate at full or part load and specify the required power levels.

5 CONCLUSIONS

This study focuses on the development of a TI-PTES model for off-design performance simulation. The model represents a 6 kWe TI-PTES unit with the specific characteristics of being a reversible HP/ORC system thermally integrated with a DHN. The objective is to develop a model that accounts for the system's boundary conditions (e.g., thermal storage temperature levels, mechanical component rotational speeds, and ambient air temperature) to predict the system's performance. Detailed component models are interconnected using the *LaboThapPy* library to simulate the entire system. After defining the boundary conditions for both HP and ORC modes, the model is used to generate performance maps. These maps serve as a guide for the initial experimental tests of the system, helping to identify unattainable zones and optimize the operating point. Future studies will validate the model through experimental tests on the test bench and refine the performance maps to establish the actual optimal operating conditions.

NOMENCLATURE

Acronyms		**Subscript**		**Variables**	
CD	Condenser	amb	ambient	$\dot{m}$	mass flow rate (kg/s)
EV	Evaporator	sf	secondary fluid	$\dot{Q}$	heat power (W)
EXP	Expander	wf	working fluid	$\dot{W}$	work power (W)
COMP	Compressor	su	supply	h	specific enthalpy (J/kg)
PP	Pump	ex	exhaust	P	pressure (bar, Pa)
LR	Liquid receiver	vlv	valve	T	temperature (K, °C)

REFERENCES

Ayub, Z. H., 'Plate Heat Exchanger Literature Survey and New Heat Transfer and Pressure Drop Correlations for Refrigerant Evaporators', Heat Transfer Engineering, vol. 24, no. 5, pp. 3–16, Sep. 2003, doi: 10.1080/01457630304056.

Bell, I. H. et al., 'A generalized moving-boundary algorithm to predict the heat transfer rate of

counterflow heat exchangers for any phase configuration', Applied Thermal Engineering, vol. 79, pp. 192–201, Mar. 2015, doi: 10.1016/j.applthermaleng.2014.12.028.

Chen, H., T. N. Cong, W. Yang, C. Tan, Y. Li, and Y. Ding, 'Progress in electrical energy storage system: A critical review', Progress in Natural Science, vol. 19, no. 3, pp. 291–312, Mar. 2009, doi: 10.1016/j.pnsc.2008.07.014.

Dickes, R., 'Charge-sensitive methods for the off-design performance characterization of organic Rankine cycle (ORC) power systems'. doi: 10.1016/j.egypro.2017.09.100.

Dickes, R., O. Dumont, L. Guillaume, S. Quoilin, and V. Lemort, 'Charge-sensitive modelling of organic Rankine cycle power systems for off-design performance simulation', Applied Energy, vol. 212, pp. 1262–1281, Feb. 2018, doi: 10.1016/j.apenergy.2018.01.004.

Dumont, O., 2017. Investigation of a heat pump reversible into an organic Rankine cycle and its application in the building sector, PhD Dissertation.

Dumont, O., C. Poletto, O. Thomé, and V. Lemort, 'Methodology for the Sizing of a Carnot Battery Based on a Rankine Cycle and Application to a 10 kWe System for District Heating Application', in 36th International Conference on Efficiency, Cost, Optimization, Simulation and Environmental Impact of Energy Systems (ECOS 2023), Las Palmas De Gran Canaria, Spain: ECOS 2023, 2023, pp. 2300–2308. doi: 10.52202/069564-0207.

Frate, G. F., L. Ferrari, and U. Desideri, 'Rankine Carnot Batteries with the Integration of Thermal Energy Sources: A Review', Energies, vol. 13, no. 18, p. 4766, Sep. 2020, doi: 10.3390/en13184766.

Hu, S., Z. Yang, J. Li, and Y. Duan, 'Thermo-economic analysis of the pumped thermal energy storage with thermal integration in different application scenarios', Energy Conversion and Management, vol. 236, p. 114072, May 2021, doi: 10.1016/j.enconman.2021.114072.

Lemort, V., Quoilin, S., Cuevas, C., Lebrun, J., 'Testing and modeling a scroll expander integrated into an Organic Rankine Cycle', Appl Therm Eng, 2009; 29(14–15): 3094–102. http://dx.doi.org/10.1016/j.applthermaleng.2009.04.013.

Neven, E., B. Chaudoir, V. Lemort, 'LaboThapPy: Development of an open-source python library for thermodynamic system modelling and simulation', 2024.

Padullés, R., M. L. Hansen, M. P. Andersen, B. Zühlsdorf, J. K. Jensen, and B. Elmegaard, 'Optimal operation of industrial heat pumps with stratified thermal energy storage for emissions and cost reduction using day-ahead predictions', Applied Thermal Engineering, vol. 266, p. 125703, May 2025, doi: 10.1016/j.applthermaleng.2025.125703.

Poletto, C., O. Dumont, A. De Pascale, V. Lemort, S. Ottaviano, and O. Thomé, 'Control strategy and performance of a small-size thermally integrated Carnot battery based on a Rankine cycle and combined with district heating', Energy Conversion and Management, vol. 302, p. 118111, Feb. 2024, doi: 10.1016/j.enconman.2024.118111.

Shah, M., 'Heat transfer during condensation in corrugated plate heat exchangers', International journal of Refrigeration, vol. 127, pp. 180–193, Jul. 2021, doi: 10.1016/j.ijrefrig.2021.02.011.

Steinmann, W.-D., D. Bauer, H. Jockenhöfer, and M. Johnson, 'Pumped thermal energy storage (PTES) as smart sector-coupling technology for heat and electricity', Energy, vol. 183, pp. 185–190, Sep. 2019, doi: 10.1016/j.energy.2019.06.058.

Tassenoy, R., O. Dumont, V. Lemort, M. D. Paepe, and S. Lecompte, 'Experimental Investigation Of A Thermally Integrated Carnot Battery Using A Reversible Heat Pump/Organic Rankine Cycle: Influence Of System Charge On Performance Of The Reversible Scroll Compressor/Expander And Global Performance', 2022.

VDI e. V., Ed., VDI Heat Atlas. Berlin, Heidelberg: Springer Berlin Heidelberg, 2010. doi: 10.1007/978-3-540-77877-6.

Weitzer, M., 'Reversible heat pump-ORC pilot plant - Experimental results and fluid charge optimization', 2023.

ACKNOWLEDGEMENT

This study was carried out in the frame of the FlexGeo project. This project is performed within the European Union's Horizon Europe research and innovation programme 787 under grant agreement No. 101147576.